ACS APPLIED MATERIALS & INTERFACES

Article

Role of Amines in Thermal-Runaway-Mitigating Lithium-ion Battery

Yang Shi, Daniel J Noelle, Meng Wang, Anh V Le, Hyojung Yoon, Minghao Zhang, Ying Shirley Meng, and Yu Qiao

ACS Appl. Mater. Interfaces, **Just Accepted Manuscript** • DOI: 10.1021/acsami.6b10501 • Publication Date (Web): 27 Oct 2016

Just Accepted

ACS Publications

ACS Applied Materials & Interfaces is published by the American Chemical Society.
1155 Sixteenth Street N.W., Washington, DC 20036

Role of Amines in Thermal-Runaway-Mitigating Lithium-ion Battery

Yang Shi,[1] Daniel J. Noelle,[1] Meng Wang,[2] Anh V. Le,[2] Hyojung Yoon,[3] Minghao Zhang,[3] Ying Shirley Meng,[1,3] Yu Qiao,[1,2,*]

[1] *Program of Materials Science and Engineering, University of California - San Diego, La Jolla, CA 92093-0418, U.S.A.*
[2] *Department of Structural Engineering, University of California - San Diego, La Jolla, CA 92093-0085, U.S.A.*
[3] *Department of NanoEngineering, University of California - San Diego, La Jolla, CA 92093-0448, U.S.A.*
[*] *Email: yqiao@ucsd.edu; Phone: +1-858-534-3388*

Abstract

Benzylamine (BA), dibenzylamine (DBA), and trihexylamine (THA) are investigated as thermal runaway retardants (TRR) for lithium-ion batteries (LIBs). In a LIB, TRR is packaged separately and released when internal shorting happens, so as to suppress exothermic reactions and slow down temperature increase. THA is identified as the most efficient TRR. Upon nail penetration, 4 wt% THA can reduce the peak temperature by nearly 50%. The working mechanisms of the three amines are different: THA is highly wettable to the separator and immiscible with the electrolyte, and therefore, it blocks lithium ion (Li^+) transport; BA and DBA decrease the ionic conductivity of electrolyte and increase the charge transfer resistance. All the three amines react with charged electrodes; the reactions of DBA and THA do not have much influence on the overall heat generation, while the reaction of BA cannot be ignored.

Keywords: Lithium-ion battery; thermal runaway; safety; conductivity; amine

1. Introduction

Because of their high specific energy and excellent cost-performance balance, lithium-ion batteries (LIBs) are promising candidates for large-scale energy storage systems, such as the battery packs in smart grids and electric vehicles. [1-2] While LIBs are generally safe and generates little heat during normal operation, once a single LIB cell is damaged, thermal runaway may happen and seriously threaten the entire structure. [3] Currently, LIB robustness and safety remains a major concern in energy storage system design.

As a LIB cell is largely deformed, its components may be broken apart, leading to the direct contact between cathode and anode and a large internal shorting current (ISC). The immense amount of energy stored in the LIBs can be released in a short period of time, accompanied by a rapid temperature rise. Once the local temperature is beyond 90-100 °C, a series of reactions among electrolyte, electrodes, and solid-electrolyte interface (SEI) layers are accelerated. [4] The electrolytes used in today's and near-future LIBs are highly volatile and flammable. [5] If they are ignited, catastrophic system failure would happen.

For a couple of decades, researchers have investigated a number of active thermal-runaway mitigation (TRM) techniques. Most of the TRM mechanisms were thermally triggered. For instance, electrodes may be modified by positive temperature coefficient (PTC) materials [6-9] or low-melting-point microspheres. [10] At 100-130 °C, the TRM additives greatly increase the internal impedance and therefore, ISC is reduced and heat generation becomes slower. A major issue is that, once the temperature is higher than 110 °C, the temperature ramp rate increases

drastically, and the thermally activated processes may not be sufficiently fast to guarantee a satisfactory safe performance of the LIB system.

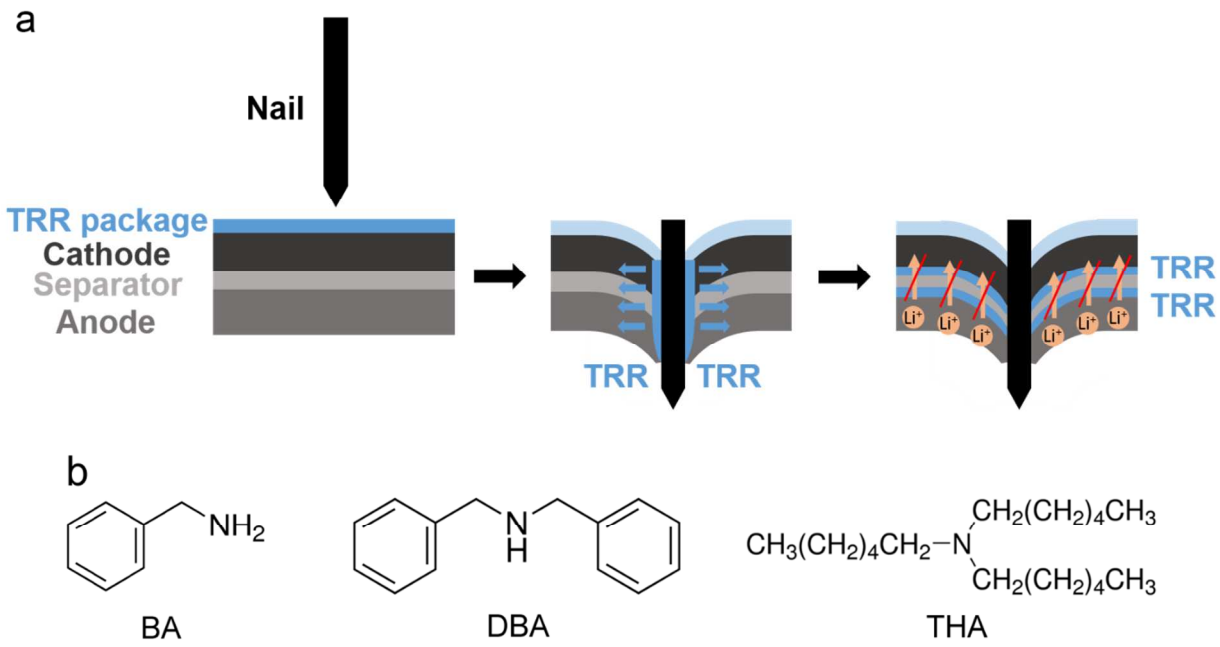

Figure 1. (a) Using TRR to mitigate thermal runaway: Left - During normal operation, TRR is sealed in a separate package; Middle - As the cell is damaged, the package ruptures and TRR is released; Right - TRR suppresses Li^+ transport and heat generation. **(b)** Chemical structures of BA, DBA and THA.

Recently, we investigated mechanically triggered TRM methods [11-13] by embedding thermal runaway retardant (TRR) packages in LIBs. [14] Upon mechanical abuse of a LIB, the TRR packages are broken apart and release TRR. A schematic is shown in **Figure 1a**. The main challenge comes from the efficiency of TRR: TRR must suppress the exothermic reactions without any sacrifice in battery capacity or large increase in mass and volume of the system. In our previous work,[14] we identified dibenzylamine (DBA) as an efficient TRR candidate. In this study, its primary amine counterpart, benzylamine (BA), and a tertiary amine, trihexylamine

(THA), are examined to understand the working mechanisms of amines. It is discovered that THA is more efficient than DBA. The chemical structures of BA, DBA and THA are depicted in **Figure 1b**.

2. Experimental Section

2.1 Nail penetration test

LIR 2450 batteries were first fully charged to 4.3 V, and then disassembled and re-assembled with open cell cases. The open cases contained two holes, which allowed for the injection of TRR. 100 μL amine (BA, DBA or THA) or pristine electrolyte was injected through the holes. The pristine electrolyte contained 1 M $LiPF_6$ in ethylene carbonate (EC) and ethyl methyl carbonate (EMC), with the EC to EMC mass ratio of 1:1, and was employed as the reference additive. Immediately after the injection, a steel nail penetrated through the cell, causing internal shorting and heating. Details of the testing procedure are similar to that of our previous work; [14] a schematic of the experimental setup is shown in supplementary **Figure S1**. The temperature of the cell was recorded by a thermocouple and the distance between the nail and the tip of thermocouple was around 7 mm.

2.2 Properties of amine-modified electrolyte

Wettability tests and contact angle measurements (KSV Instruments CAM 100) were carried out by dropping 50 μL electrolyte or amine on trilayer

Polypropylene/Polyethylene/Polypropylene (PP/PE/PP) separator (Celgard 2320). The conductivities of the electrolytes with various BA or DBA concentrations were recorded by a conductivity meter.

To evaluate the influence of amines on cell resistance, 2016 coin cells were made following the procedure established previously.[14] Cathode was composed of $LiNi_{0.5}Co_{0.2}Mn_{0.3}O_2$, carbon black, and polyvinylidene fluoride, with the mass ratio of 93:3:4. The cells were assembled with lithium disks as anodes, and PP/PE/PP membranes as separators. Electrochemical impedance spectroscopy (EIS) measurements were carried out on the cells assembled with pristine electrolyte (1M $LiPF_6$ in EC:EMC 1:1) and electrolyte containing 5 wt% BA or DBA.

High-performance liquid chromatography (HPLC) analysis was performed on a Jupiter Proteo90A Phenomenex Column using a Hitachi-Elite LaChrome L-2130 pump equipped with a UV-Vis Detector. Buffer A was 0.1% trifluoroacetic acid (TFA) in water and Buffer B was 99.9% acetonitrile (ACN) and 0.1 % TFA. Mass spectra of products from HPLC were recorded by Thermo LCQdeca. Fourier transform infrared spectroscopy (FTIR) measurements were performed using Bruker ALPHA FTIR Spectrometer from 4000 to 450 cm^{-1}. FTIR analysis of the mixtures of EC-EMC solvent modified by different amount of BA or DBA was carried out after the components were homogenized by magnetic stirring for 30 mins. 0.1 g $LiPF_6$ had been added to 1 mL BA or DBA, followed by 30 min magnetic stirring and passing through a 200-nm pore-size PTFE filter to remove undissolved $LiPF_6$. FTIR analysis of the filtered solution was then performed.

2.3 Interaction of amines with electrodes

Cathode and anode films were separately harvested from fully charged LIR 2450 cells. 100 μL amime (BA, DBA or THA) was dropped onto the electrodes and the local temperature was measured.

2016 coin cells were made according to the procedure in Section 2.2 and charged to 4.3 V at 20 mA g^{-1} after resting for 2 hours. The cathode disks from disassembled charged cells were rinsed with dimethyl carbonate (DMC) in the glovebox, and divided into three groups. The first group of cathode disks were soaked in 15 mL selected amine for 20 min, followed by thorough rinsing with DMC. New coin cells were made with the rinsed cathodes and lithium disk anodes; the cells were discharged to 3 V at 20 mA g^{-1} after resting for 2 hours. The second group of cathode disks were also soaked in selected amine, followed by thorough rinsing with DMC, and then analyzed using X-ray Photoelectron Spectroscopy (XPS) (Kratos AXIS Supra) with Al K_{α} radiation. The spectra were calibrated by assigning the C 1s peak at 284.6 eV. For the third group, 50 mg charged cathode disks were soaked in 0.5 mL BA, DBA or THA for 20 min and then mass spectra of the amine phases were recorded by a the same mass spectrometer to detect the reaction products.

3. Results and Discussion

The amine injection immediately before the nail penetration simulates the working process of TRR: During normal operation of a LIB cell, TRR is sealed in non-permeable packages, separated from electrodes and electrolyte; when the cell is damaged, TRR packages rupture and TRR is released into the cell, simultaneously as internal shorting takes place. In the current research, the TRR amount is kept as 4 wt% of the total weight of cathode, anode, electrolyte and separator.

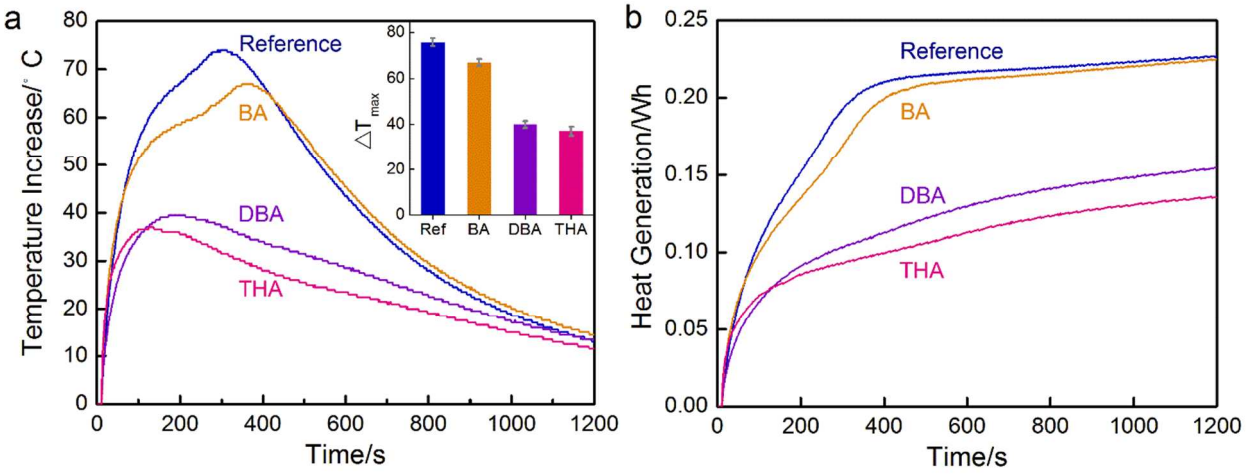

Figure 2. (a) Nail penetration test temperature profiles on the reference and amine-modified cells; the inset shows the maximum temperatures increase. **(b)** Calculated heat generation of the reference and amine-modified batteries

Figure 2a shows the temperature profiles of the cells influenced by TRR. Among the three amines, BA has the least effect on the maximum temperature increase (ΔT_{max}); THA is the most efficient one to reduce ΔT_{max}, better than DBA. [14] Addition of THA reduces ΔT_{max} by about 50%, from ~75 °C in reference cells to ~36 °C. **Figure 2b** shows the calculated heat generation in the first 20 minutes after nail penetration, using an analytical model that accounts for convective

heat transfer and ignores radiative heat transfer. [14] 4 wt% THA results in about 45% reduction in heat generation, from ~0.23 Wh in reference cells to ~0.13 Wh.

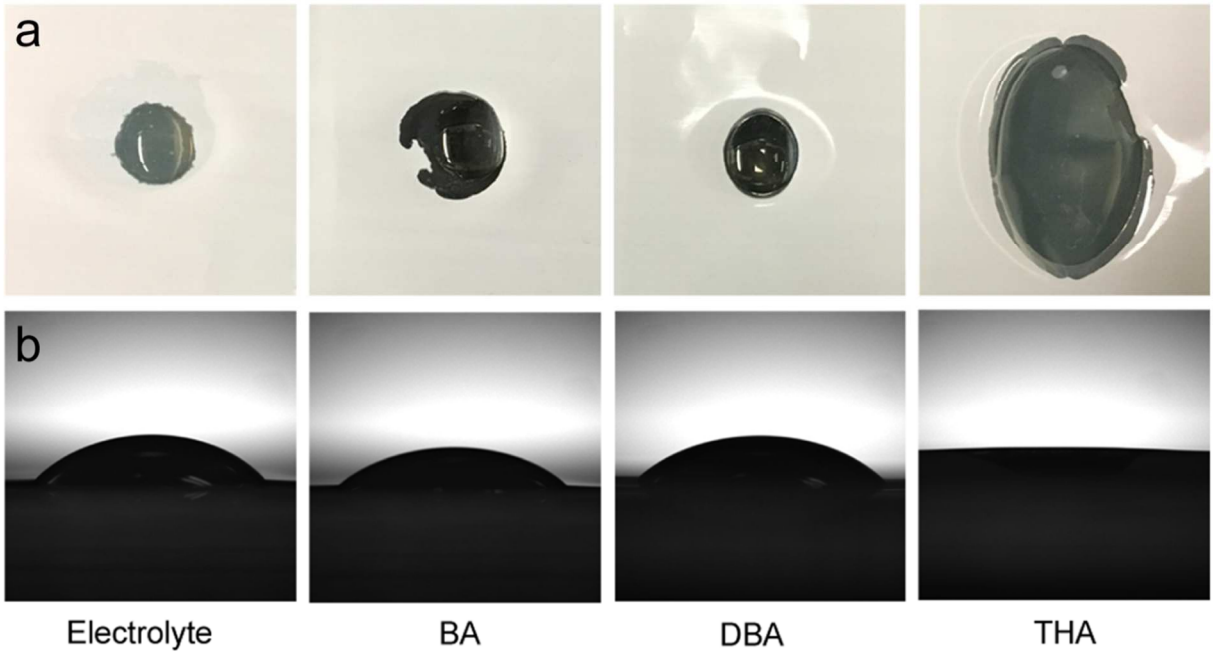

Figure 3. (a) Top view and **(b)** side view of contact angle measurement of electrolyte and amines.

The three amines under investigation, namely BA, DBA, and THA, represent primary, secondary, and tertiary amines, respectively. They have different effects on ΔT_{max}, which should be related to both of their physical and chemical properties. BA and DBA are miscible with electrolyte while THA is not; the latter enables THA to form a blocking layer between cathode and anode, using the porous separator as the scaffold. Wettability testing results (**Figure 3a**) indicate that in a given period of time, THA can spread over a much larger area on separator than electrolyte, BA, and DBA. The contact angle measurement further confirms that THA is by far the most wettable liquid to the separator (**Figure 3b**). Thus, when THA is released into LIB, it rapidly disperses in the separator and displaces the electrolyte in the separator pores, forming a

physical barrier between the electrodes, such that Li^+ transport is suppressed. As the internal impedance largely rises, ISC decreases, so does the heat generation.

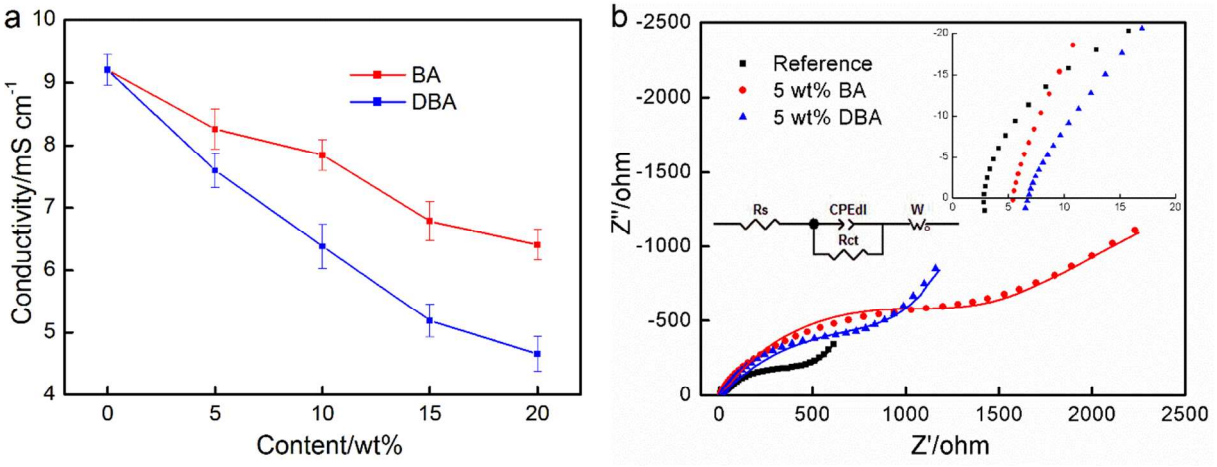

Figure 4. (a) Conductivities of BA and DBA modified electrolytes. **(b)** EIS measurement results of reference, BA-modified, and DBA-modified cells; the inset displays the plots at an enlarged scale

Both BA and DBA are miscible with electrolyte and therefore, cannot physically block ion transport; however, they reduce the ionic conductivities of electrolyte. As shown in **Figure 4a**, when more BA or DBA is added, the electrolyte conductivity decreases monotonously. With the same amount of amine, DBA can reduce the electrolyte conductivity more efficiently than BA. **Figure 4b** displays the EIS measurement results of the coin cells assembled with pristine and BA or DBA modified electrolytes, in which R_s is the electrolyte resistance and R_{ct} is the charge transfer resistance. [15] **Table 1** shows the resistance values extracted from the fitting results. While the BA-modified cell has a lower electrolyte resistance, it has a larger charge transfer resistance than the DBA modified cell.

Table 1. Resistance values in EIS measurement

	Reference (Ω)	BA (Ω)	DBA (Ω)
R_s	2.81	5.43	6.76
R_{ct}	395	997	802

The reduction in conductivity of BA or DBA modified electrolyte may be caused by the influence of amine on either the solvent (EC and EMC) or the solute ($LiPF_6$), or both. Amines can attack the carbonyl carbon in EC, followed by ring-opening that gives a urethane product. [16] BA-EC and DBA-EC reactions are proposed, as displayed in **Figure 5a** and **Figure 5b**. HPLC is used to separate the possible reaction products between amines and electrolyte solvent; it shows that both BA and DBA react with EC while neither of them reacts with EMC (Supplementary **Figure S2a** and **Figure S2b**). The mass spectra results (Supplementary **Figure S3a** and **Figure S3b**) show that the molecular weights of BA-EC and DBA-EC reaction products are as expected in **Figure 5a** and **Figure 5b**, which confirms the proposed reaction mechanism. FTIR measurements are carried out to demonstrate the BA-EC and DBA-EC reactions. **Figure 6a** shows the FTIR spectra of neat BA, EC-EMC solution, and their mixtures. The bands corresponding to the C=O stretching vibration mode of the EC molecule are observed at 1774 cm^{-1} and 1799 cm^{-1}, in which the 1774 cm^{-1} band is attributed to the C=O stretching and the 1799 cm^{-1} band to the overtone of the ring breathing mode. [17] The 1743 cm^{-1} band is attributed to the C=O stretching vibration mode of the EMC molecule. [17] As BA is added to the EC-EMC solution, the bands at 1774 cm^{-1} and 1799 cm^{-1} become weaker and a new band at 1707 cm^{-1} shows up. The new band is attributed to the urethane carbonyl group. [18] With the increasing amount of BA, the carbonate absorption bands (1774 cm^{-1} and 1799 cm^{-1}) disappear and are

replaced by the urethane carbonyl band. **Figure 6b** shows the FTIR spectra of neat DBA, EC-EMC solution, and their mixtures. Compared with **Figure 6a**, as DBA is added to the EC-EMC solution, the C=O stretching mode of EC does not disappear and no new band is observed, which is consistent with the HPLC analysis (Supplementary **Figure S2b**). Clearly, according to the HPLC analysis and the FTIR spectra, BA-EC reaction is more aggressive than the DBA-EC reaction.

When BA and electrolyte is mixed, white precipitates gradually appear, accompanied by heat generation, which should be associated with the $LiPF_6$-catalyzed exothermic polymerization of EC. [19] The reaction mechanism is displayed in **Figure 5c**. Such phenomena are not observed in the DBA-electrolyte mixture.

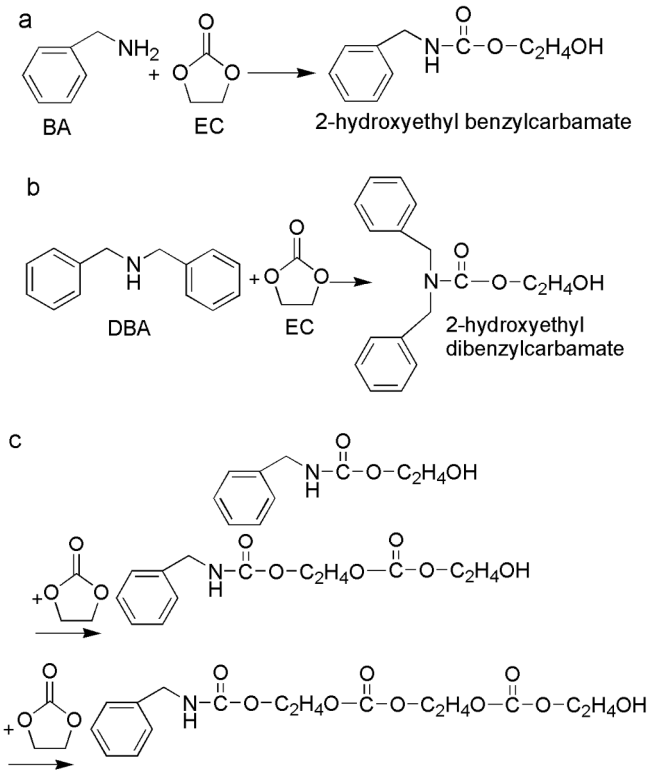

Figure 5. Proposed reaction mechanisms of **(a)** BA and EC, **(b)** DBA and EC, and **(c)** $LiPF_6$ catalyzed EC polymerization.

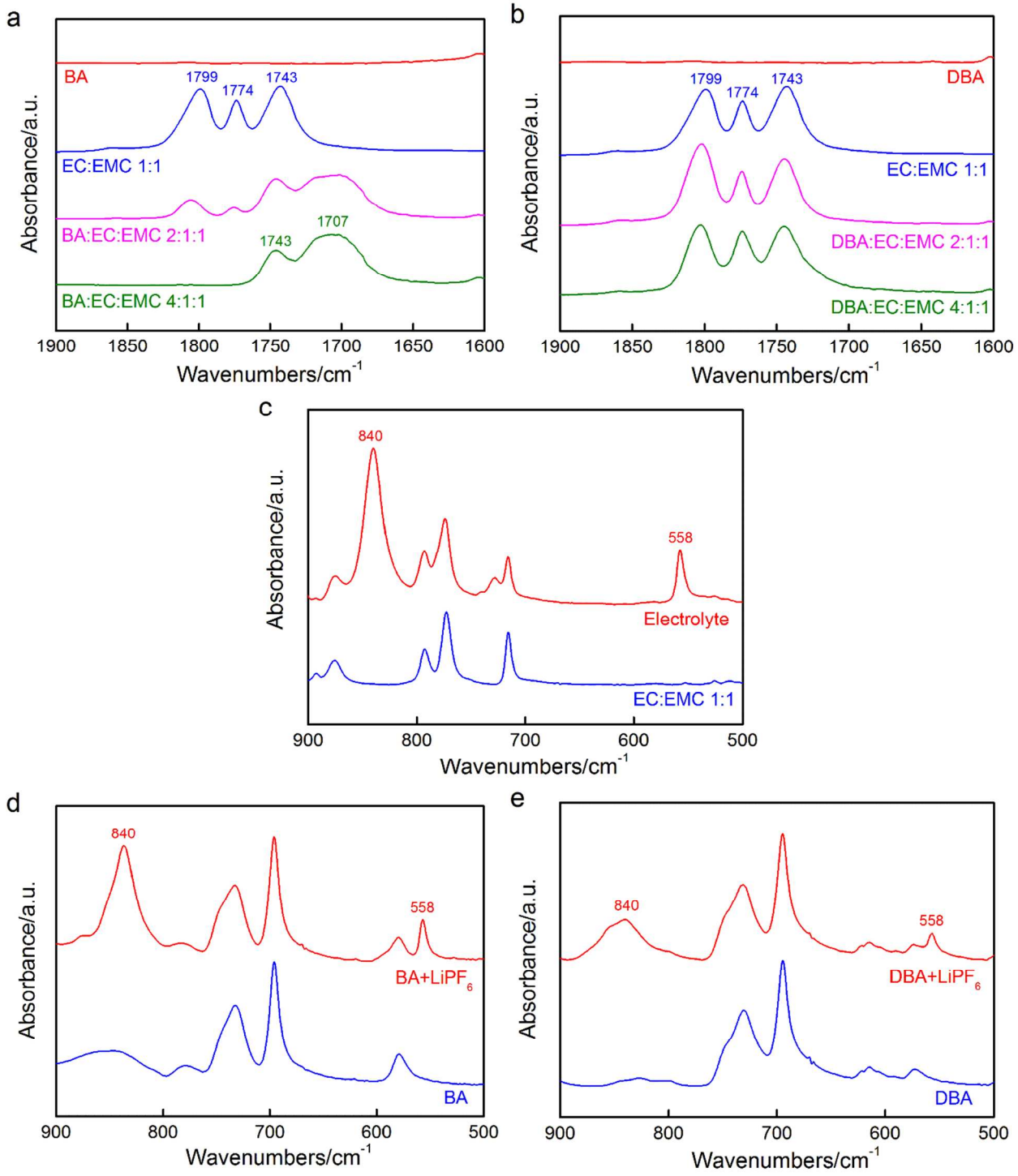

Figure 6. FTIR spectra of **(a)** BA, EC-EMC solvent, and their mixtures; **(b)** DBA, EC-EMC solvent, and their mixtures; **(c)** electrolyte and EC-EMC solvent; **(d)** BA and $LiPF_6$; and **(e)** DBA and $LiPF_6$.

When $LiPF_6$ is added in BA or DBA, it disappears. There are two possible mechanisms: 1) dissolution of $LiPF_6$ in amines and 2) chemical reactions of amines and $LiPF_6$. The FTIR spectra of electrolyte and EC-EMC are compared in **Figure 6c** and the two bands that appear in electrolyte while not in EC-EMC are attributed to the P-F vibrations in PF_6^-. [20] The band at 840 cm^{-1} and 558 cm^{-1} correspond to the P-F stretching and bending mode, respectively. [21] The FTIR measurements of BA-$LiPF_6$ and DBA-$LiPF_6$ mixtures are carried out after the undissolved $LiPF_6$ is removed, as shown in **Figure 6d** and **Figure 6e**. The two bands at 850 cm^{-1} and 558 cm^{-1} match the same vibrations as the PF_6^- anion in the electrolyte, suggesting that $LiPF_6$ is dissolved in BA or DBA. If $LiPF_6$ reacted with BA or DBA, the octahedral symmetry of the PF_6^- anion must have been destroyed and the P-F stretching and bending modes should have changed.

As shown in **Figure 4a**, adding BA or DBA in electrolyte leads to a reduction in ionic conductivity, which may be due to their dissolution of $LiPF_6$, according to the previous discussion. The donor number (DN) and the dielectric constant (ε) of the solvents play important roles in the solvation process. [22] **Table 2** displays the DN and ε values of BA, DBA, EC and EMC. [23-25] BA and DBA are strong Lewis bases and have larger DN than EC. The carbonyl oxygens of EC are the binding sites for Li^+ and their lone-pair electrons could effectively neutralize the coulombic attraction of Li^+. [26] The solvation shell of Li^+ would be broken apart when a cosolvent of higher DN is present. [27] BA and DBA would compete with EC on the solvation of Li^+; however, they have much smaller dielectric constants than EC and EC-EMC mixture, which means they are poor dissociating solvents. The dissociation of Li^+ and PF_6^- pairs increases the number of free Li^+, which helps increase the electrolyte conductivity. [28] That is,

poor dissociating solvents such as BA and DBA may perturb the original Li^+ solvation shells and decrease the overall electrolyte conductivity.

Table 2. Donor number and dielectric constant values at 25 ℃

	BA	DBA	EC	EMC	EC:EMC (1:1)
Donor number (kcal/mol)	40	50	16.4	17.2	—
Dielectric constant	4.6	3.6	95.3	3.5	33.6

It is noticed that the addition of DBA leads to a larger reduction in electrolyte conductivity than addition of the same amount of BA (**Figure 4a**), which correlates well with the fact that the DBA-EC reaction is less intense than the BA-EC reaction. The consumption of EC by BA or DBA may not be the main reason for the reduction in electrolyte conductivity, since EC/EMC based electrolyte solvent has existing EC-EMC mass ratio of 3:7. Due to the intense reaction between BA and EC, BA is considerably consumed and the remaining BA for solvation perturbation is reduced, so that the extent of reduction in electrolyte conductivity is lowered.

As different amines are dropped on the cathodes and anodes harvested from fully charged (4.3 V) LIR 2450 cells, local temperatures are monitored continuously and the results are displayed in **Figure 7a**. For charged anodes, upon exposure to BA, there is a slight temperature increase, which may be due to the reactions between BA and SEI. There is no temperature change when the charged anodes are exposed to DBA or THA. For charged cathodes, abrupt temperature increase is observed upon exposure to BA, DBA or THA. After the cathodes are fully rinsed to remove any remaining amines, they are reassembled with fresh pristine

electrolyte. The discharge capacities of the reference, BA, DBA or THA modified cells are 164 mAh g^{-1}, 27.2 mAh g^{-1}, 149.2 mAh g^{-1} and 157.1 mAh g^{-1}, respectively (**Figure 7b**). The initial voltage drop of the reference cell results from the voltage relaxation. Amine-treated cathodes have larger voltage drops than the reference cathode, probably because of the redox reactions between amines and charged cathode. The charged cathode could oxidize the primary amine into oxime [29], benzylidenebenzylamine [30] or dibenzyldiazene [31], as shown in **Figure 7c**. Benzaldehyde oxime is solid at room temperature, which could be formed on the surface of charged cathode. The latter two are liquid and their molecular weight is confirmed by mass spectra (Supplementary **Figure S4**). Secondary and tertiary amines could be oxidized into imine or amine oxides [32], and the reaction products are solid, which could also form on the surface of the charged cathode (**Figure 7d** and **Figure 7e**). No liquid reaction products are detected in the mass spectra of DBA and THA. For DBA and THA, the solid products on the surface could prevent further reactions between the charged cathodes and amines, so that the discharge capacities of DBA and THA treated cathodes are comparable with that of the reference cell. In general, capacity losses and voltage drops of amine treated cathodes are due to the combination of cathode degradation and formation of resistive layers on electrode surfaces.

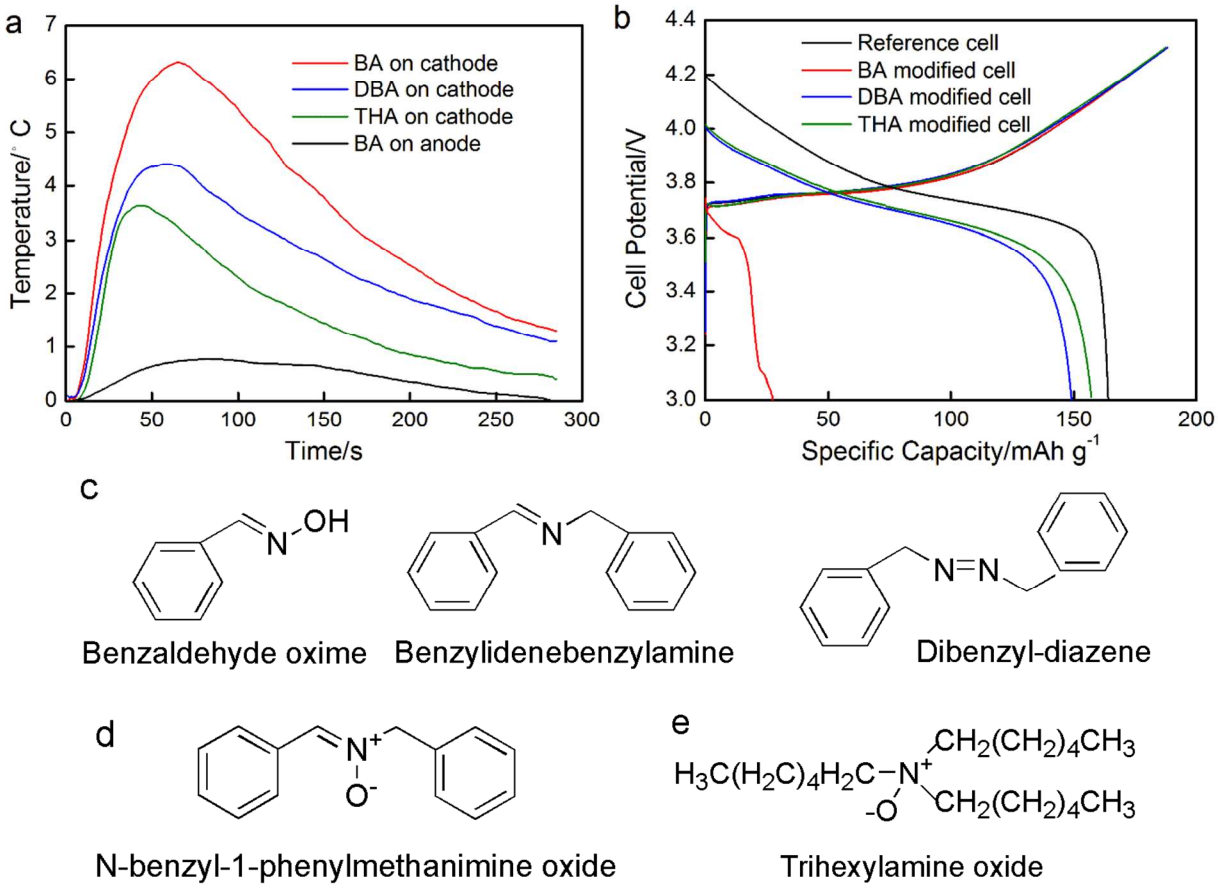

Figure 7. (a) Temperature changes of cathodes and anodes exposed to amines. **(b)** Charge-discharge plots of the reference and amine-modified cells. Reaction products between charged cathode and **(c)** BA, **(d)** DBA, and **(e)** THA.

To confirm the existence of resistive organic layers, XPS spectra are obtained on the surface of the amine-treated cathodes, as shown in **Figure 8**. N 1s peak at 399.7 eV is observed on reference cathode not treated by amines, which must be the residue from the electrolyte precipitating on cathode surface since there is no nitrogen element in cathodes. For BA treated cathode, the new component at 401.4 eV is attributed to C=N in benzaldehyde oxime. [33] There is a small amount of solid reaction product between BA and charged cathodes and most of the reaction products are liquid (Supplementary **Figure S4**), which explains the large decrease in discharge capacity of BA treated cathode, because the reactions could happen continuously

without any barrier layers. The peaks at 400.9 eV for DBA treated cathode and 401.9 eV for THA treated cathode are attributed to $C=N^+$ in imine oxide and $C\text{-}N^+$ in amine oxide, respectively. [34-35] In the C 1s spectra (**Figure 8b**), the peaks assigned at 286.1 eV (C-H) and 290.7 eV (C-F) are related to the PVDF binder. [36] The peak corresponding to carbon black is observed at 284.6 eV (C-C). The peaks at 287.2 eV and 289.1 eV are assigned to C-O in carbonate salts and C=O in lithium alkyl carbonates, respectively. [37] For amines treated cathode, new C 1s peaks appear at 285.5 eV, 285.7 eV and 285.8 eV, which is attributed to C=N, $C=N^+$ and $C\text{-}N^+$ bonds in oxime, imide oxide and amine oxide, respectively. [38] It is noticed that the C-H and C-F bonds in PVDF shift to higher binding energies for all amine treated cathode. This is due to the reaction of amines with PVDF binders, since PVDF is sensitive to bases that can degrade it by creating insaturations. [39] The binding energy of C-C also shifts in amine treated cathodes. In the O 1s spectra (**Figure 8c**), besides the peaks for C-O (533.0 eV) and C=O (531.1 eV), the peak at 529.4 eV is assigned to the bonds between transition metals and oxygen. [40-41] Amine treated cathodes have extra peaks at 530.5 eV (N-O), 531.7 eV ($N^+\text{-}O^-$) and 531.0 eV ($N^+\text{-}O^-$), which is consistent with the N 1s and C 1s spectra. The difference of the two $N^+\text{-}O^-$ peaks at 531.7 eV and 531.0 eV might be due to the different chemical environment of nitrogen (**Figure 7d** and **Figure 7e**). The XPS patterns of amine treated cathode proves that organic resistive layers form on cathode surfaces, which might also correlate with the increased R_{ct} in the EIS measurements (**Figure 4b**).

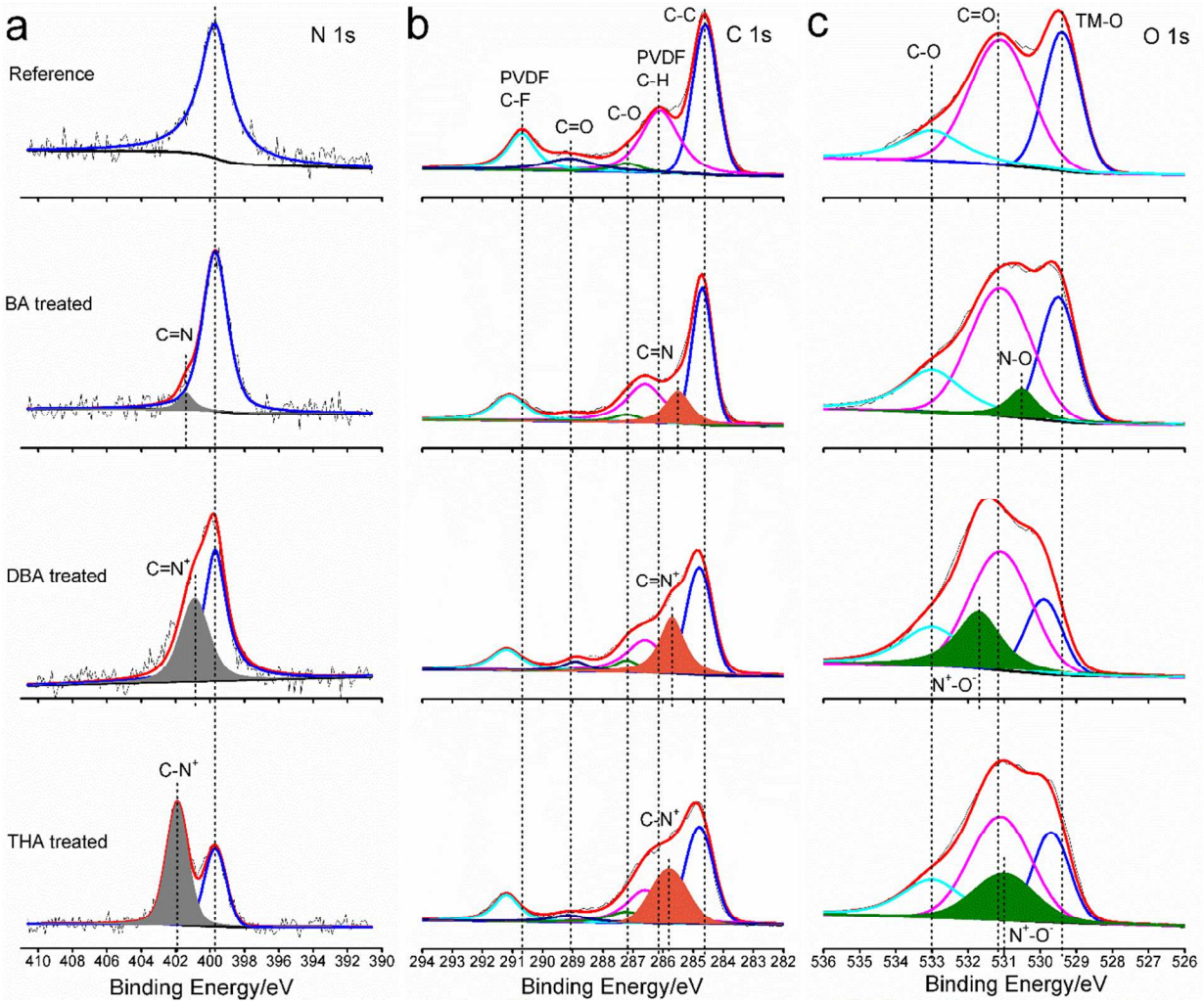

Figure 8. XPS patterns of reference and amine-treated cathodes: **(a)** N 1s **(b)** C 1s **(c)** O 1s

Coin cells based on DBA or THA treated cathodes have 91% and 96% of the capacity of reference cathode, and it is clear that the reactions between amines and cathode are exothermic (**Figure 7a**). Therefore, the cathode-DBA and cathode-THA reactions should not play a significant role in the generation of heat during nail penetration. The perturbation of the Li^+ solvation shell by DBA and the physical barrier layer formed by THA on separator are the main factors in heat generation reduction. For BA, it is clear that there is an intense reaction between BA and charged cathodes. On the one hand, the reaction generates heat, while on the other hand,

it decreases cathode voltage. The combination of the perturbation of Li^+ solvation shell by BA and the interactions of BA with charged cathode leads to the slight reduction in ΔT_{max}.

The heat generation of LIB cell may be described by an exponential function.[3,4] When the temperature is below 110 °C, the heat is generated mainly from the galvanic reactions and the mild temperature increase could be balanced by heat dissipation. However, when the temperature is higher than 110 °C, exothermic chemical reactions between electrodes and electrolyte accelerate. Compared to thermally triggered TRM mechanisms which begins to function only after the heating rate starts to drastically increase, a mechanically triggered TRM method takes effect at room temperature. By suppressing the Li^+ transport after TRR is released, the galvanic reactions is inhibited. If temperature can be kept below 110 °C, no aggressive exothermic reactions could take place.

This mechanically triggered method can be potentially applied to large-sized pouch cells, by embedding TRR packages in electrodes or attaching them on the inner surface of pouch cell cases. The design of geometry, material, size, and spacing of TRR packages is crucial to the cost efficiency and scalability, which will be a crucial topic of our future research.

4. Conclusions

To summarize, three different amines, BA, DBA and THA, are investigated as thermal-runaway retardants (TRR) for lithium-ion batteries (LIBs). They respectively represent primary, secondary, and tertiary amines. The efficiency of thermal-runaway mitigation of THA is the

highest, and that of BA is the lowest. In nail penetration test, 4 wt% THA decreases the maximum temperature rising of charged LIR 2450 cells by ~50%. The working mechanisms of the three amines are different. THA has a high wettability to the separator and can displace electrolyte, and therefore, forms a barrier that blocks lithium ion transport. Both BA and DBA decrease the electrolyte ionic conductivity and elevate the charge transfer resistance. The exothermic reactions between charged cathodes and DBA or THA are not dominant factors of the decreased heat generation in nail penetration test. The exothermic reactions between charged cathode and BA is intense, and contributes to the overall heat generation.

Supporting Information

Nail penetration test setup. HPLC analysis of BA, DBA, EC, EMC and their mixtures. Mass spectra of the reaction products of EC with BA or DBA, and BA with the charged cathode.

Acknowledgement

This research is supported by Advanced Research Projects Agency - Energy (ARPA-E) under Grant No. DE-AR0000396, for which we are grateful to Dr. Ping Liu, Dr. John Lemmon, Dr. Grigorii Soloveichik, Dr. Chris Atkinson, and Dr. Dawson Cagle.

References

1. Etacheri, V.; Marom, R.; Elazari, R.; Salitra, G.; Aurbach, D., Challenges in the Development of Advanced Li-Ion Batteries: a Review. *Energy Environ. Sci.* **2011,** *4*, 3243-3262.

2. Thackeray, M. M.; Wolverton, C.; Isaacs, E. D., Electrical Energy Storage for Transportation-Approaching the Limits of, and Going Beyond, Lithium-Ion Batteries. *Energy Environ. Sci.* **2012,** *5*, 7854-7863.

3. Finegan, D. P.; Scheel, M.; Robinson, J. B.; Tjaden, B.; Hunt, I.; Mason, T. J.; Millichamp, J.; Di Michiel, M.; Offer, G. J.; Hinds, G.; Brett, D. J. L.; Shearing, P. R., In-Operando High-speed Tomography of Lithium-Ion Batteries during Thermal Runaway. *Nat. Commun.* **2015,** *6*, 6924.

4. Balakrishnan, P. G.; Ramesh, R.; Prem Kumar, T., Safety Mechanisms in Lithium-Ion Batteries. *J. Power Sources* **2006,** *155*, 401-414.

5. Ohmi, N.; Nakajima, T.; Ohzawa, Y.; Koh, M.; Yamauchi, A.; Kagawa, M.; Aoyama, H., Effect of Organo-Fluorine Compounds on the Thermal Stability and Electrochemical Properties of Electrolyte Solutions for Lithium Ion Batteries. *J. Power Sources* **2013,** *221*, 6-13.

6. Feng, X. M.; Ai, X. P.; Yang, H. X., A Positive-Temperature-Coefficient Electrode with Thermal Cut-off Mechanism for Use in Rechargeable Lithium Batteries. *Electrochem. Commun.* **2004,** *6*, 1021-1024.

7. Zhong, H.; Kong, C.; Zhan, H.; Zhan, C.; Zhou, Y., Safe Positive Temperature Coefficient Composite Cathode for Lithium Ion Battery. *J. Power Sources* **2012,** *216*, 273-280.

8. Li, J.; Chen, J. G.; Lu, H.; Jia, M.; Jiang, L. X.; Lai, Y. Q.; Zhang, Z. A., A Positive-Temperature-Coefficient Layer Based on Ni-Mixed Poly(Vinylidene Fluoride) Composites for $LiFePO_4$ Electrode. *Int. J. Electrochem. Sci.* **2013,** *8*, 5223-5231.

9. Zhang, H.; Pang, J.; Ai, X.; Cao, Y.; Yang, H.; Lu, S., Poly(3-Butylthiophene)-Based Positive-Temperature-Coefficient Electrodes for Safer Lithium-Ion Batteries. *Electrochim. Acta* **2016,** *187*, 173-178.

10. Baginska, M.; Blaiszik, B. J.; Merriman, R. J.; Sottos, N. R.; Moore, J. S.; White, S. R., Autonomic Shutdown of Lithium-Ion Batteries Using Thermoresponsive Microspheres. *Adv. Energy Mater.* **2012,** *2*, 583-590.

11. Le, A. V.; Wang, M.; Shi, Y.; Noelle, D.; Qiao, Y.; Lu, W., Effects of Additional Multiwall Carbon Nanotubes on Impact Behaviors of $LiNi_{0.5}Mn_{0.3}Co_{0.2}O_2$ Battery Electrodes. *J. Appl. Phys.* **2015,** *118*, 085312.

12. Le, A. V.; Wang, M.; Shi, Y.; Noelle, D. J.; Qiao, Y., Heat Generation of Mechanically Abused Lithium-Ion Batteries Modified by Carbon Black Micro-Particulates. *J. Phys. D: Appl. Phys.* **2015,** *48*, 385501-385507.

13. Wang, M.; Le, A. V.; Noelle, D. J.; Shi, Y.; Yoon, H.; Zhang, M.; Meng, Y. S.; Qiao, Y., Effects of Electrode Pattern on Thermal Runaway of Lithium-Ion Battery. *Int. J. Damage Mech.* **2016**, 1056789516660176.

14. Shi, Y.; Noelle, D. J.; Wang, M.; Le, A. V.; Yoon, H.; Zhang, M.; Meng, Y. S.; Qiao, Y., Exothermic Behaviors of Mechanically Abused Lithium-Ion Batteries with Dibenzylamine. *J. Power Sources* **2016,** *326*, 514-521.

15. Ni, J.; Zhou, H.; Chen, J.; Zhang, X., Improved Electrochemical Performance of Layered $LiNi_{0.4}Co_{0.2}Mn_{0.4}O_2$ via Li_2ZrO_3 Coating. *Electrochim. Acta* **2008,** *53* (7), 3075-3083.

16. Clements, J. H., Reactive Applications of Cyclic Alkylene Carbonates. *Ind. Eng. Chem. Res.* **2003,** *42*, 663-674.

17. Ikezawa, Y.; Nishi, H., In Situ FTIR Study of the Cu Electrode/Ethylene Carbonate + Dimethyl Carbonate Solution Interface. *Electrochim. Acta* **2008,** *53*, 3663-3669.

18. Mahmood, N.; Khan, A. U.; Sohail Khan, M.; Ali, Z.; Haq, A.U.; Wutzler, A., In Situ FT-IR-ATR Studies on the Structure Development of Polyurethane-Urea Systems. *J. Appl. Polym. Sci.* **2011,** *122*, 1012-1018.

19. Gnanaraj, J. S.; Zinigrad, E.; Asraf, L.; Gottlieb, H. E.; Sprecher, M.; Schmidt, M.; Geissler, W.; Aurbach, D., A Detailed Investigation of the Thermal Reactions of $LiPF_6$ Solution in Organic Carbonates Using ARC and DSC. *J. Electrochem. Soc.* **2003,** *150*, A1533-A1537.

20. Kock, L. D.; Lekgoathi, M. D. S.; Crouse, P. L.; Vilakazi, B. M., Solid State Vibrational Spectroscopy of Anhydrous Lithium Hexafluorophosphate ($LiPF_6$). *J. Mol. Struct.* **2012,** *1026*, 145-149.

21. Yang, H.; Zhuang, G. V.; Ross Jr, P. N., Thermal Stability of $LiPF_6$ Salt and Li-Ion Battery Electrolytes Containing $LiPF_6$. *J. Power Sources* **2006,** *161*, 573-579.

22. Sekhon, S. S.; Arora, N.; Singh, H. P., Effect of Donor Number of Solvent on the Conductivity Behaviour of Nonaqueous Proton-Conducting Polymer Gel Electrolytes. *Solid State Ionics* **2003,** *160*, 301-307.

23. Marcus, Y., The Effectivity of Solvents as Electron Pair Donors. *J. Solution Chem.* **1984,** *13*, 599-624.

24. Hall, D. S.; Self, J.; Dahn, J. R., Dielectric Constants for Quantum Chemistry and Li-Ion Batteries: Solvent Blends of Ethylene Carbonate and Ethyl Methyl Carbonate. *J. Phys. Chem. C* **2015,** *119*, 22322-22330.

25. Maryott, A. A.; Smith, E. R., Table of Dielectric Constants of Pure Liquids. *Circ. Natl. Bur. Stand.* **1951,** *C514*, 44

26. Takeuchi, M.; Matubayasi, N.; Kameda, Y.; Minofar, B.; Ishiguro, S.i.; Umebayashi, Y., Free-Energy and Structural Analysis of Ion Solvation and Contact Ion-Pair Formation of Li^+ with $BF4^-$ and $PF6^-$ in Water and Carbonate Solvents. *J. Phys. Chem. B* **2012,** *116*, 6476-6487. **2012,** *116* (22), 6476-6487.

27. Xu, K., Electrolytes and Interphases in Li-Ion Batteries and Beyond. *Chem. Rev.* **2014,** *114*, 11503-11618.

28. Sun, X.; Lee, H. S.; Yang, X. Q.; McBreen, J., Comparative Studies of the Electrochemical and Thermal Stability of Two Types of Composite Lithium Battery Electrolytes Using Boron-Based Anion Receptors. *J. Electrochem. Soc.* **1999,** *146*, 3655-3659.

29. Suzuki, K.; Watanabe, T.; Murahashi, S.-I., Oxidation of Primary Amines to Oximes with Molecular Oxygen using 1,1-Diphenyl-2-picrylhydrazyl and WO_3/Al_2O_3 as Catalysts. *J. Org. Chem.* **2013,** *78*, 2301-2310.

30. Khusnutdinov, R. I.; Baygusina, A. R.; Aminov, R. I., Synthesis of N-Benzylidenebenzylamine from Benzylamine under the Action of Iron-Containing Catalysts in CCl_4. *Russ. J. Org. Chem.* **2012,** *48*, 1059-1061.

31. Biradar, A. V.; Kotbagi, T. V.; Dongare, M. K.; Umbarkar, S. B., Selective N-Oxidation of Aromatic Amines to Nitroso Derivatives Using a Molybdenum Acetylide Oxo-Peroxo Complex as Catalyst. *Tetrahedron Lett.* **2008,** *49*, 3616-3619.

32. Colladon, M.; Scarso, A.; Strukul, G., Mild Catalytic Oxidation of Secondary and Tertiary Amines to Nitrones and N-Oxides with H_2O_2 Mediated by Pt(ii) Catalysts. *Green Chem.* **2008,** *10*, 793-798.

33. Wang, F.; Li, H.; Liu, Q.; Li, Z.; Li, R.; Zhang, H.; Liu, L.; Emelchenko, G. A.; Wang, J., A Graphene Oxide/Amidoxime Hydrogel for Enhanced Uranium Capture. *Sci. Rep.* **2016,** *6*, 19367.

34. Choudhury, D.; Das, B.; Sarma, D. D.; Rao, C. N. R., XPS Evidence for Molecular Charge-Transfer Doping of Graphene. *Chem. Phys. Lett.* **2010,** *497*, 66-69.

35. Peng, H.; Mo, Z.; Liao, S.; Liang, H.; Yang, L.; Luo, F.; Song, H.; Zhong, Y.; Zhang, B., High Performance Fe- and N- Doped Carbon Catalyst with Graphene Structure for Oxygen Reduction. *Sci. Rep.* **2013,** *3*, 1765.

36. Lee, J.; Choi, W., Surface Modification of Over-Lithiated Layered Oxides with PEDOT:PSS Conducting Polymer in Lithium-Ion Batteries. *J. Electrochem. Soc.* **2015,** *162*, A743-A748.

37. Yang, L.; Ravdel, B.; Lucht, B. L., Electrolyte Reactions with the Surface of High Voltage $LiNi_{0.5}Mn_{1.5}O4$ Cathodes for Lithium-Ion Batteries. *Electrochem. Solid-State Lett.* **2010,** *13*, A95-A97.

38. Park, S. S.; Chu, S.W.; Xue, C.; Zhao, D.; Ha, C.S., Facile Synthesis of Mesoporous Carbon Nitrides Using the Incipient Wetness Method and the Application as Hydrogen Adsorbent. *J. Mater. Chem.* **2011,** *21*, 10801-10807.

39. A. Taguet, B. A., Bernard Boutevin, Crosslinking of Vinylidene Fluoride-Containing Fluoropolymers. *Adv. Polym. Sci.* **2005,** *184*, 127-211.

40. Bodenes, L.; Dedryvere, R.; Martinez, H.; Fischer, F.; Tessier, C.; Peres, J. P., Lithium-Ion Batteries Working at 85 degrees C: Aging Phenomena and Electrode/Electrolyte Interfaces Studied by XPS. *J. Electrochem. Soc.* **2012,** *159*, A1739-A1746.

41. Lin, F.; Nordlund, D.; Markus, I. M.; Weng, T.C.; Xin, H. L.; Doeff, M. M., Profiling the Nanoscale Gradient in Stoichiometric Layered Cathode Particles for Lithium-Ion Batteries. *Energy Environ. Sci.* **2014,** *7*, 3077-3085.

For Table of Contents Only